Journal of Thermal Analysis and Calorimetry, Vol. 95 (2009) 1, 81–86

SOLID SOLUTIONS IN THE $MgO–Al_2O_3–Cr_2O_3$ SYSTEM
Effects of polymorphism, temperature and pressure

A. I. Turkin[1] *and V. A. Drebushchak*[1,2]*

[1]Institute of Geology and Mineralogy SB RAS, Pr. Ak. Koptyuga, 3, Novosibirsk 630090, Russia
[2]Novosibirsk State University, Ul. Pirogova 2, Novosibirsk 630090, Russia

Coexisting solid solutions with spinel and corundum structure were synthesized at 1773 K and two pressures, 1 bar and 25 kbar. Samples were analyzed by electron microprobe analysis and X-ray powder diffraction.

Pressure and temperature were shown to affect the properties of the solid solutions in different ways. Pressure governs the composition of the defect spinel $Mg_{1-x}Al_2O_4$, and temperature changes the cation distribution between coexisting phases. This allows one to separate the effects of cation exchange and magnetic contribution to the heat capacity in thermodynamic modeling. The defect spinel itself can form only because γ-Al_2O_3 exists, polymorph with spinel structure.

Thermodynamic considerations argue in favor of eskolaite-spinel assemblages prevailing over corundum–picrochromite ones at very high temperatures deep in the Earth.

Keywords: *corundum, phase diagram, solid solutions, spinel, thermodynamics*

Introduction

Crystalline phases in the $MgO–Al_2O_3–Cr_2O_3$ system are refractory materials. This is a reason why their relationships between composition and properties are investigated intensively for many decades. Solid solutions in the $MgO–Al_2O_3–Cr_2O_3$ system make the phase relations among them quite complicated [1], and broaden the investigations into other systems, for example, iron-bearing ones [2]. Cation distribution between $MgAl_2O_4$–$MgCr_2O_4$ spinel solid solution (ssS) and Al_2O_3–Cr_2O_3 solid solution with corundum structure (ssC) was investigated in metallurgy [3, 4]. Such an approach allows one to derive the activity of components and treat the solid solutions using ideal or slightly non-ideal models.

Recently magnetic contribution to the heat capacity of corundum–eskolaite solid solutions was investigated and found to be irregular function of composition [5]. In conventional thermodynamic models with activities, this irregularity would corrupt the model thermodynamic functions significantly, yielding large discrepancy between calculated and experimental values. Heat capacity of spinel-picrochromite solid solutions was also investigated, but magnetic contribution was not evaluated [6]

Solid solutions in the $MgO–Al_2O_3–Cr_2O_3$ system are of great importance in geoscience, because chromium is considered the element of the assemblages deep in the Earth. Nevertheless, defect spinel in the $MgO–Al_2O_3$ system was the main subject of such investigations for a long time, aimed at the refinement of the data received in material science [7, 8].

The subject of this work was to investigate the relation between spinel solid solutions and 'corundum' solid solutions in the $MgO–Al_2O_3–Cr_2O_3$ system under ambient and elevated pressure in order to clarify the mechanism of the defect spinel formation and cation distribution between the solid solutions.

Experimental

Samples

Samples with intermediate compositions were synthesized from oxides Al_2O_3, Cr_2O_3 and MgO of 'high purity' grade. End-member spinels, $MgAl_2O_3$ and $MgCr_2O_3$, were synthesized at 1 atm and 1873 K, heating duration about 60 h [9]. They were used as starting materials for the synthesis of solid solutions at the central part of the phase diagram (see below). Composition of the mixtures for the synthesis is indicated in Tables 1 and 2 in letters and numbers as follows. For example, sample S80P20-C80E20 contains the oxides equivalent to 0.8 mole of spinel ($MgAl_2O_3$)+0.2 picrochromite ($MgCr_2O_3$)+0.8 corundum (Al_2O_3)+0.2 eskolaite (Cr_2O_3), total $1MgO+1.6Al_2O_3+0.4Cr_2O_3$. Sample mass in a batch was about 100 mg.

* Author for correspondence: dva@uiggm.nsc.ru

1388–6150/$20.00

Akadémiai Kiadó, Budapest, Hungary
Springer, Dordrecht, The Netherlands

Table 1 Composition (mass%) of solid solutions in the $MgO–Al_2O_3–Cr_2O_3$ system after the experiment at 1 bar and 1773 K

Sample		MgO	Al_2O_3	Cr_2O_3	Total
S50-C50	ssS	20.6	76.9	2.2	99.7
S10P90-C10E90	ssS	24.9	9.4	64.2	98.5
S20P80-C20E80	ssS	23.9	19.7	55.4	99.0
S30P70-C30E70	ssS	25.4	30.2	43.0	98.6
S40P60-C40E60	ssS	23.6	32.8	40.2	96.6
S40P60-C40E60	ssC	0.3	35.5	61.4	97.1
S60P40-C60E40	ssS	24.9	47.3	27.1	99.3
S60P40-C60E40	ssC	0.3	63.6	36.7	100.6
S70P30-C70E30	ssS	24.1	56.0	17.6	97.6
S80P20-C80E20	ssS	21.9	66.2	12.1	100.1
S90P10-C90E10	ssS	21.3	71.3	6.7	99.3
P50-C50	ssS	23.9	35.3	37.1	96.3
S50-E50	ssS	26.4	33.2	36.5	96.0

Synthesis

Experiments under ambient pressure were carried out in a shaft furnace with Silit heaters and temperature control. All samples were synthesized together, in a single experiment at 1773 K for 19 days. Crucibles with the mixtures were covered with lids to protect the samples from solid impurities falling into crucibles, but not protecting from gas phase. As chromium oxide is volatile at high temperatures, it escapes from samples with elevated Cr_2O_3 content and penetrates into neighbor crucibles, increasing the Cr_2O_3 content there. It was readily detected after the experiment due to the red (ruby) shade of samples without initial impurity of chromium oxide (green itself). Microprobe analysis proved these observations, indicating the increase in the Cr_2O_3 content of the product as compared with the starting material.

Experiments at 1773 K and 25 kbar were carried out in the high-pressure 'piston-cylinder' apparatus with NaCl cells. Usually, only one sample was synthesized in one experiment, each for 15 h in a hermetically closed Pt crucible. The procedure was described elsewhere [10].

To ensure the equilibrium composition of products, 'two-side' approach was used. Mixtures in the central part of the phase diagram were prepared in two ways, $MgAl_2O_4+Cr_2O_3$ and $MgCr_2O_4+Al_2O_3$. The samples were sealed in separate Pt crucibles, placed in one cell, and heated together in the single run. The products (spinel solid solution $MgAlCrO_4$ and 'corundum' solid solution $AlCrO_3$) were analyzed, and their cation distribution was found to be the same within the limits of the experimental error.

Methods

Microprobe analysis

Experimental phases were analyzed with CAMECA MS46 electron microprobe with an energy-dispersive analyzer. Accelerating voltage was of 15 kV, the beam current 20 nA, and the counting time 100 s. Six to ten analyses were carried out for each phase.

X-ray powder diffraction

X-ray patterns were studied using a DRON-3 X-ray diffractometer with CuK_α radiation in the range of $22°<2\Theta<96°$ at a counter rate of 0.5° min^{-1}. High purity silicon was used as an internal standard (cell parameter a_0=5.43088 Å). Silicon was added in an amount allowing us to detect the doublets α_1 and α_2 of

Table 2 Averaged composition (mass%) and the unit cell parameters of ssS and ssC in the $MgO–Al_2O_3–Cr_2O_3$ system after the experiments at 25 kbar and 1773 K

Sample		MgO	Al_2O_3	Cr_2O_3	Total	*a*/nm	*c*/nm
S90P10-C90E10	ssS	27.57	58.64	14.42	100.63	0.81193(3)	
S90P10-C90E10	ssC	0.24	92.56	6.61	99.40	0.47713(7)	1.30276(48)
S70P30-C70E30	ssS	26.71	42.02	31.80	100.52	0.81750(3)	
S70P30-C70E30	ssC	0.15	72.82	26.84	99.81	0.48117(3)	1.31158(10)
S50-E50	ssS	25.25	32.40	42.00	99.64	0.82072(4)	
S50-E50	ssC	0.18	39.14	59.96	99.27	0.48665(13)	1.32654(49)
P50-C50	ssS	25.47	31.00	42.71	99.18	0.82084(5)	
P50-C50	ssC	0.19	37.66	61.70	99.54	0.48677(5)	1.32838(17)
S30P70-C30E70	ssS	25.74	20.06	53.57	99.37	0.82481(2)	
S30P70-C30E70	ssC	0.18	16.64	82.43	99.25	0.49139(6)	1.34315(27)
S10P90-C10E90	ssS	23.02	6.76	70.89	100.67	0.83036(2)	
S10P90-C10E90	ssC	0.25	4.55	95.63	100.43	0.49485(3)	1.35486(9)

its least intensive reflection (400). Correction was determined by seven reflections not overlapping with the reflections of the phases studied. If the scatter of the correction values determined by these reflections did not exceed 0.01° (2Θ), average value was used as the correct value, otherwise the correction was introduced as a linear function of the 2Θ angle. The cell parameters of synthesized phases were calculated using the method of least squares.

Results and discussion

1 bar

Results of the microprobe analysis of the samples synthesized in the experiments under ambient pressure are listed in Table 1 (in mass%). Recalculated in the mole percentage, the results are shown in Fig. 1. In the discussion below, we will pay attention to (1) the violation of stoichiometry of the spinel solid solution (ssS) in the Al-rich (i.e., left) side and (2) the direction of tie-lines in the middle of the triangle. Chromium impurity decreases the deviation from stoichiometric composition. Under ambient pressure and 1773 K, the ssS should be considered stoichiometric for Cr/(Cr+Al)≥0.3.

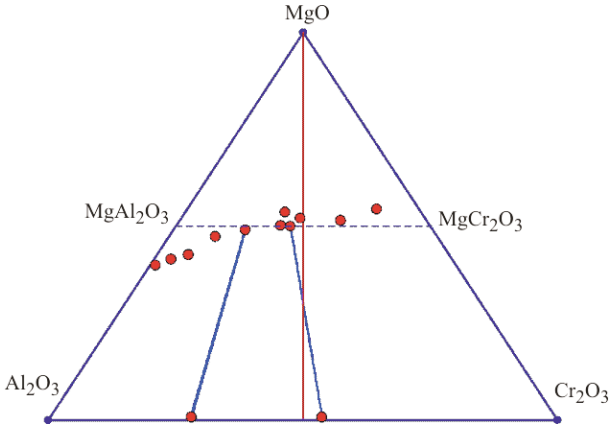

Fig. 1 Results of the experiment at 1773 K and 1 bar. Vertical line in the middle of the diagram is the eye guide for the tie-line rotation

25 kbar

Composition of the ssS and ssC synthesized in the experiments under 25 kbar and 1773 K are listed in Table 2 (in mass%). Recalculated in the mole percentage, the results are shown in Fig. 2. Spinel is close to stoichiometry, even for the samples with the least Cr_2O_3 content. Unit cell parameters for the ssS (cubic, a_0) and the ssC (a and c for the hexagonal setting) are also listed in Table 2.

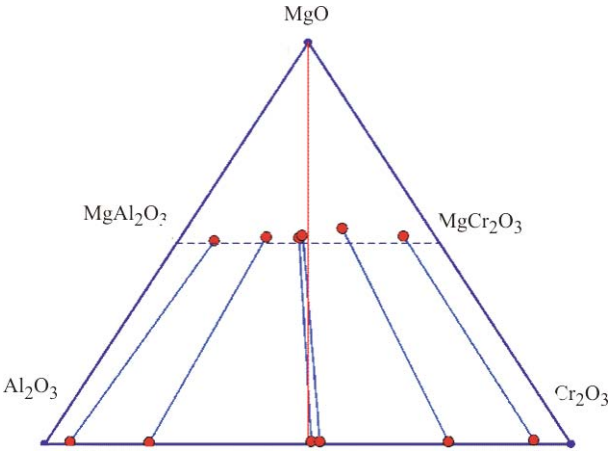

Fig. 2 Results of the experiments at 1773 K and 25 kbar

Non-stoichiometric spinel

Non-stoichiometric Al-rich spinel at 1 bar is the most significant effect of pressure if we compare the phase diagrams in Figs 1 and 2. Such an effect is absent for Cr-rich ssS. The reason of the difference between Al-rich ssS and Cr-rich ssS is not in the properties of the end-member spinels themselves, i.e., $MgAl_2O_3$ and $MgCr_2O_3$, but in the properties of their counterparts in the phase equilibrium, i.e., Al_2O_3 and Cr_2O_3.

There are many polymorphs of Al_2O_3: cubic γ and η, tetragonal δ, orthorhombic δ and κ, hexagonal χ, trigonal α (stable under ambient conditions), monoclinic θ, θ', θ", and γ [11]. Cubic γ polymorph with the spinel structure is very important for our discussion. Its composition is indicated often as $Al_{2.67}O_4$, but formula $Al_{2/3}Al_2O_4$ describes its crystal chemistry much better. Isostructural phases $MgAl_2O_3$ and $Al_{2/3}Al_2O_4$ form solid solutions according to the scheme of cation substitution 3Mg↔2Al. Total number of cations in the solid solution is less than that in stoichiometric spinel (Me:O=3:4). The more the fraction of γ-Al_2O_3 in the solid solution, the less the number of cations, and the more defects in the solid solution.

Mixing spinel with corundum, we prepare the starting material for the solid solution. But the solid solution is formed only between isostructural phases, and the reaction consists of two stages:

$$\alpha\text{-}Al_2O_3 \leftrightarrow (1\text{-}x)\alpha\text{-}Al_2O_3 + x\gamma\text{-}Al_2O_3 \quad (=Al_{2/3}Al_2O_4) \qquad (1a)$$

$$MgAl_2O_4 + xAl_{2/3}Al_2O_4 \leftrightarrow (1+x)Mg_{1/(1+x)}Al_{2x/3(1+x)}Al_2O_4 \qquad (1b)$$

At the first stage, stable trigonal α-polymorph transforms partly into unstable 'spinel' γ-Al_2O_3. At the second stage, two phases with spinel structure interact, yielding the solid solution, i.e., defect spinel. Combining Eqs (1a) and (1b), we have:

$$\alpha\text{-}Al_2O_3+MgAl_2O_4 \leftrightarrow$$
$$(1-x)\alpha\text{-}Al_2O_3+(1+x)Mg_{1/(1+x)}Al_{2x/3(1+x)}Al_2O_4 \quad (2)$$

Net reaction looks like the reaction between corundum and spinel because α-Al_2O_3 is spent and the solid solution is produced.

Corundum is more dense than γ-Al_2O_3: d=3.977 [12] and 3.653 [13], respectively. The increase in pressure makes both intermediate reagent (γ-Al_2O_3) and product (defect spinel) more unstable, suppressing reaction (2). Here, pressure affects as the $P\Delta V$ term in the Gibbs function ($\Delta G=\Delta U+P\Delta V-T\Delta S$), adding significant (about 5 kJ mol^{-1}) positive contribution.

Oxides Al_2O_3 and Fe_2O_3 exemplify the key role of isostructural end-members. γ-Al_2O_3 is a purchased chemical for the preparation of various blends with other unstable reagents [14]. Like Al_2O_3, Fe_2O_3 forms several polymorphs. Stable polymorph is α-Fe_2O_3 (hematite) with corundum-like structure. Corundum-hematite solid solutions, i.e., the ssC, are among natural minerals. Metastable γ-Fe_2O_3 with the spinel structure also exists [15, 16]. Besides metastable γ-Fe_2O_3, there is another iron oxide with the spinel structure, Fe_3O_4. These two minerals can form the ssS Fe_3O_4–$Fe_{2.67}O_4$, defect iron spinel. And finally, variations in the parameters of the reaction between Al_2O_3 and Fe_2O_3 can produce both solid solutions, the ssS and ssC [17].

Oxide with the spinel structure does not exist in the system Cr–O. At least, we failed to find the references with its structure and/or unit cell parameters. Thus, counterpart '$Cr_{2/3}Cr_2O_4$' for reaction $MgCr_2O_4+xCr_{2/3}Cr_2O_4$ does not exist. First stage (1a) in the reaction producing the defect spinel is absent for Cr-rich spinel, and it remains stoichiometric. Several models were published, where the properties of defect picrochromite are calculated using hypothetical spinels Cr_2O_3 and Cr_3O_4 [18], but no reliable experimental data on these phases were found in literature.

Cation distribution between ssS and ssC

Difference in the Cr/Al content between the ssS and ssC is represented in Figs 1 and 2 with tie-lines. Alternatively, it can be plotted as the distribution coefficient. Writing $Mg(Al_{1-x}Cr_x)_2O_4$ for the ssS and $(Al_{1-y}Cr_y)_2O_3$ for the ssC, one can plot the Cr mole fraction in the ssS as a function of the Cr mole fraction in the ssC, i.e., x *vs.* y. Such a way of data presentation is very useful in the numerical modeling of phase equilibrium. Here, we will use qualitative consideration. Tie-lines are more visual and suitable for our purposes [19].

The tie-lines in the middle of the phase diagrams shown in Figs 1 and 2 are turned slightly counter-clockwise ($x<y$), crossing the vertical line ($x=y=0.5$). The direction of the rotation is different in [4], where the experiments were carried at 1473 K. Tie-lines for $0<y<0.6$ are rotated clockwise ($x>y$). Of three tie-lines determined at 1573 K [3], one near the Al_2O_3-rich side is almost parallel to that obtained at 1473 K. The directions of the other two tie-lines are quite different. These were considered incorrect because the composition of the ssC was derived from the unit cell parameters [4], not measured directly.

We measured the compositions using the electron microprobe analysis, and our tie-lines rotate counter-clockwise even more significantly than in [3]. We think, the data in [3] were in fact correct. The reason of the changes in the tie-lines rotation is in the thermodynamics of the ssS and ssC.

After the emf measurements [20, 21], the difference in the Gibbs energy for reaction

$$Cr_2O_3+MgAl_2O_4=Al_2O_3+MgCr_2O_4 \quad (3)$$

was found to change with temperature as

$$\Delta G=-21600+11.27T\pm570 \text{ J mol}^{-1} \quad (4)$$

For $\Delta G<0$, the products of the reaction are on the right-hand side, and we have corundum+picrochromite. For $\Delta G>0$, the products are on the left-hand side, with eskolaite+spinel. In fact, the products of this reaction are solid solutions, the ssS and ssC, not pure minerals. In accurate thermodynamic evaluation, one should consider thermodynamic data for the ssS and ssC as a function of temperature, pressure, and composition. For example, enthalpy and entropy of Cr_2O_3 have magnetic contributions ΔH_m and ΔS_m as compared with Al_2O_3. At high temperatures, when eskolaite is paramagnetic, these contributions tends to the constant values. In the Gibbs energy ($\Delta G=\Delta H-T\Delta S$), magnetic contribution is with sign '–' due to the product $T\Delta S$, increasing with temperature. The greater temperature, the less the Gibbs energy on the left-hand side of Eq. (3). We investigated this contribution for several samples of the ssC and can now evaluate the magnetic contribution to the Gibbs function of the ssC [5]. Unfortunately, data on magnetic contribution to the heat capacity of the ssS were not derived from the C_P [6].

Let us consider small changes in the composition of coexisting ssS and ssC, with Δ as the amount of cations exchanged:

$$(Al_{1-y-\Delta}Cr_{y+\Delta})_2O_3+Mg(Al_{1-x+\Delta}Cr_{x-\Delta})_2O_4=$$
$$(Al_{1-y+\Delta}Cr_{y-\Delta})_2O_3+Mg(Al_{1-x-\Delta}Cr_{x+\Delta})_2O_4 \quad (5)$$

Cr-enriched ssC and Cr-depleted ssS are on the left-hand side, while Cr-depleted ssC and Cr-enriched ssS are on the right-hand side. If the Gibbs function decreases after the reaction ($\Delta G<0$), the tie-line turns clockwise as compared with $(Al_{1-y}Cr_y)_2O_3+Mg(Al_{1-x}Cr_x)_2O_4$. Contrary, if the

Gibbs function increases after the reaction ($\Delta G>0$), the tie-line turns counter-clockwise.

This change in the direction of tie-lines is shown in Fig. 4 for the middle of the phase diagram ($x=y=0.5$). Taking formally $\Delta=0.5$, we transform Eq. (5) into (3). Let us consider the latter again, now applying its properties to the solid solutions. The difference in the Gibbs function for Eq. (3) changes with temperature. It is negative for low temperatures (the tie-line turns clockwise) and positive for high temperatures (counter-clockwise), with zero at 1917±51 K. Considering temperature affecting pure phases and solid solutions in a similar way, we anticipate that ΔG in reaction (5) will change its sign from '–' to '+' somewhere near 1900 K and the tie-lines turn from clockwise to counter-clockwise. Inspecting Figs 1 to 3, we see that the tie-lines actually rotate from clockwise to counter-clockwise with increasing temperature. The greatest clockwise rotation ($\Delta G<0$) is for 1473 K [4]. It remains clockwise, but with a less slope, for 1573 K [3]. And finally, the tie-lines turn counter-clockwise ($\Delta G>0$) at 1773 K, both for 1 bar and 25 kbar. The difference in the Gibbs energy in reaction (5) does change in sign between 1600 and 1700 K.

It is very interesting, that the pressure itself does not affect the cation distribution between the ssS and ssC essentially. Tie-lines in Figs 1 and 2 differ insignificantly from one another. This result concerns directly to petrology, because it means that the eskolaite-spinel assemblages will prevail over corundum-picrochromite ones at the elevated temperatures deep in the Earth.

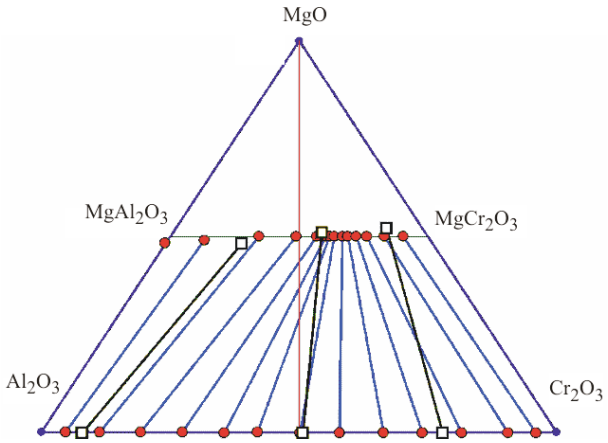

Fig. 3 Literature data on the MgO–Al_2O_3–Cr_2O_3 system: □ – 1573 K [3] and ● – 1473 K [4]

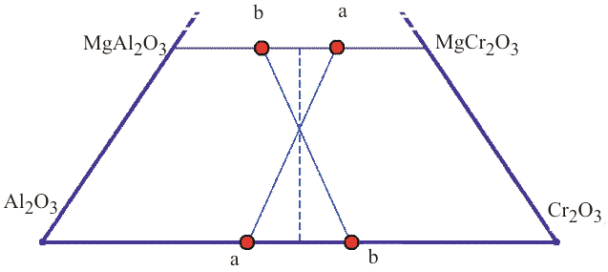

Fig. 4 Tie-lines between the ssS and ssC in the middle of the phase diagram depending on ΔG for reaction (5): a – $\Delta G<0$ and b – $\Delta G>0$

Conclusions

Phase diagram of the MgO–Al_2O_3–Cr_2O_3 system was investigated in the two-phase region of coexisting $MgAl_2O_4$–$MgCr_2O_4$ and Al_2O_3–Cr_2O_3 solid solutions at 1773 K and two pressures, 1 bar and 25 kbar.

Defect spinel $Mg_{1-x}Al_2O_4$ is shown to exist because cubic γ-Al_2O_3 with spinel structure exists. As there is no Cr_2O_3 polymorph with spinel structure, picrochromite does not form defect spinel and remains stoichiometric in the metal-to-oxygen ratio.

Cation distribution between the ssS and ssC changes with temperature, causing the tie-lines to rotate from clockwise to counter-clockwise. The reason is not in the incorrect experiments, as it was supposed in literature, but in the changes of the Gibbs energy for the reaction of cation exchange. This result will be used for the development of thermodynamic model of coexisting solid solutions with cation exchange, together with the data on magnetic contribution to the heat capacity of corundum-eskolaite solid solution.

Acknowledgements

The work was supported with RFBR grants (06-05-65114 and 05-05-64556). The authors thank Dr. Tatiana N. Drebushchak for the valuable discussion on the X-ray data for the polymorphs in the MgO–Al_2O_3-Cr_2O_3 system.

References

1 A. M. Alper, R. N. McNally, P. H. Ribbe and R. C. Doman, J. Am. Ceram. Soc., 45 (1962) 263.
2 Ya. V. Klyucharov, Yu. D. Kuznetsov and S. A. Suvorov, Refract. Ind. Ceram., 11 (1970) 380.
3 M. Hino, K. Higuchi, T. Nagasaka and S. Ban-ya, Iron Steel Inst. Jpn., 35 (1995) 851.
4 K. T. Jacob and C. K. Behera, Metall. Mater. Trans., B31 (2000) 1323.
5 V. A. Drebushchak and A. I. Turkin, J. Therm. Anal. Cal., 90 (2007) 795.
6 S. Klemme and M. Ahrens, Phys. Chem. Miner., 34 (2007) 59.
7 H. U. Viertel and F. Seifert, Neues Jb. Miner. Abh., 134 (1979) 167.
8 H. U. Viertel and F. Seifert, Neues Jb. Miner. Abh., 140 (1980) 89.
9 A. I. Turkin, Experimental Investigations on Upper Mantle, IGG SB AS USSR, Novosibirsk 1982, p. 44.

10 A. I. Turkin, I. V. Ashchepkov and A. M. Doroshev, Geol. Geofiz., 38 (1997) 1165.
11 I. Levin and D. Brandon, J. Am. Ceram. Soc., 81 (1998) 1995.
12 M. J. Cooper, Acta Cryst., B38 (1982) 264.
13 R.-S. Zhou and R. L. Snyder, Acta Cryst., B47 (1991) 617.
14 J. Zhang, J. L. Zeng, Y. Y. Liu, L. X. Sun, F. Xu, W. S. You and Y. Sawada, J. Therm. Anal. Cal., 91 (2008) 189.
15 A. N. Shmakov, G. N. Kryukova, S. V. Tsybulya, A. L. Chuvilin and L. P. Solov'eva, J. Appl. Cryst., 28 (1995) 141.
16 Y. Ichiyanagi and Y. Kimishima, J. Therm. Anal. Cal., 69 (2002) 919.
17 M. D. C. Prieto, J. M. G. Amores, V. S. Escribano and G. Busca, J. Mater. Chem., 4 (1994) 1123.
18 I.-H. Jung, S. Decterov and A. D. Pelton, J. Am. Ceram. Soc., 88 (2005) 1921.
19 B. Cheynet, D. Barbier and S. Ricoud, J. Therm. Anal. Cal., 90 (2007) 333.
20 K. T. Jacob, J. Electrochem. Soc., 124 (1977) 1827.
21 K. T. Jacob, K. P. Jaydevan and Y. Waseda, J. Am. Ceram. Soc., 81 (1998) 209.

Received: March 1, 2008
Accepted: May 19, 2008
OnlineFirst: August 15, 2008

DOI: 10.1007/s10973-008-9083-2